J|A|C|S
ARTICLES

Published on Web 03/06/2009

# Plasmonic $Cu_{2-x}S$ Nanocrystals: Optical and Structural Properties of Copper-Deficient Copper(I) Sulfides

Yixin Zhao,[†] Hongcheng Pan,[†,‡] Yongbing Lou,[†] Xiaofeng Qiu,[†] JunJie Zhu,[*,‡] and Clemens Burda[*,†]

*Center for Chemical Dynamics and Nanomaterials Research, Department of Chemistry, Case Western Reserve University, 10900 Euclid Avenue, Cleveland, Ohio 44106, and Key Laboratory of Analytical Chemistry for Life Science Department of Chemistry, Nanjing University, Nanjing 210093, P. R. China*

Received July 20, 2008; E-mail: burda@case.edu; jjzhu@netra.nju.edu.cn

***Abstract:*** $Cu_{2-x}S$ ($x = 1$, 0.2, 0.03) nanocrystals were synthesized with three different chemical methods: sonoelectrochemical, hydrothermal, and solventless thermolysis methods in order to compare their common optical and structural properties. The compositions of the $Cu_{2-x}S$ nanocrystals were varied from CuS (covellite) to $Cu_{1.97}S$ (djurleite) through adjusting the reduction potential in the sonoelectrochemical method, adjusting the pH value in the hydrothermal method and by choosing different precursor pretreatments in the solventless thermolysis approach, respectively. The crystallinity and morphology of the products were characterized by X-ray diffraction (XRD) and transmission electron microscopy (TEM), which shows that most of them might be of pure stoichiometries but some of them are mixtures. The obtained XRDs were studied in comparison to the XRD patterns of previously reported $Cu_{2-x}S$. We found consistently that under ambient conditions the copper deficient $Cu_{1.97}S$ (djurleite) is more stable than $Cu_2S$ (chalcocite). Corroborated by recent computational studies by Lambrecht et al. and experimental work by Alivisatos et al. This may be the reason behind the traditionally known instability of the bulk $Cu_2S$/CdS interface. Both $Cu_2S$ and the copper-deficient $Cu_{1.97}S$ have very similar but distinguishable electronic and crystal structure. The optical properties of these $Cu_{2-x}S$ NCs were characterized by UV−vis spectroscopy and NIR. All presented $Cu_{2-x}S$ NCs show a blue shift in the band gap absorption compared to bulk $Cu_{2-x}S$. Moreover the spectra of these $Cu_{2-x}S$ NCs indicate direct band gap character based on their oscillator strengths, different from previously reported experimental results. The NIR spectra of these $Cu_{2-x}S$ NCs show a carrier concentration dependent plasmonic absorption.

## Introduction

Since the discovery of CdS/$Cu_2S$ heterojunction solar cells in 1954,[1] copper sulfides have drawn a lot of attention as an important component in photovoltaic cells.[2,3] Copper sulfides ($Cu_{2-x}S$) can vary their band gap and structure with varying stoichiometries. The stoichiometric factor (2-x) in $Cu_{2-x}S$ varies in a wide range between 1 and 2, from the Cu-rich $Cu_2S$ (chalcocite) to CuS (covellite). Intermediate phases include $Cu_{1.97}S$ (djurleite), $Cu_{1.8}S$ (digenite), $Cu_{1.4}S$ (anilite) and others have been produced. These $Cu_{2-x}S$ nanocrystals can be used as p-type semiconductor due to the copper vacancies in the lattice, which is the reason for their use in optoelectronic devices.[4,5] Most recent theoretical work has studied the electronic structure of these interesting different copper sulfides.[6] The results showed that there is no evidence for an indirect band gap in hexagonal $Cu_{2-x}S$, which is distinctly different from previous reports.[4] Due to the attractive applications and an attempt to better understand these $Cu_{2-x}S$, a lot of methods have been developed for the synthesis of nanostructured copper sulfides.[5,7−15] Lou et al. used a single source precursor method to decompose $Cu(S_2CNEt_2)_2$ in a TOP/TOPO/TOPS solvent system to obtain spherical $Cu_{1.8}S$ (digenite) nanocrystals.[5,16−18] Klimov et al. used a topochemical method to obtain copper sulfide nanoparticles.[19] Ghezelbash et

[†] Case Western Reserve University.
[‡] Nanjing University.

(1) Reynolds, D. C.; Leies, G.; Anter, L. L.; Margurber, R. E. *Phys. Rev.* **1954**, *96*, 533–534.
(2) Chopra, K. L.; Das, S. R. *Thin Film Solar Cells*; Plenum Press: New York, 1983.
(3) Neville, R. C. *Solar Energy Conversion: The Solar Cell*; Elsevier: Amsterdam, 1995.
(4) Partain, L. D.; Mcleod, P. S.; Duisman, J. A.; Peterson, T. M.; Sawyer, D. E.; Dean, C. S. *J. Appl. Phys.* **1983**, *54*, 6708–6720.
(5) Lou, Y. B.; Samia, A. C. S.; Cowen, J.; Banger, K.; Chen, X. B.; Lee, H.; Burda, C. *Phys. Chem. Chem. Phys.* **2003**, *5*, 1091–1095.
(6) Lukashev, P.; Lambrecht, W. R. L.; Kotani, T.; van Schilfgaarde, M. *Phys. Rev. B* **2007**, *76*, 195202/1–195202/14.
(7) An, C. H.; Wang, S. T.; He, J.; Wang, Z. X. *J. Cryst. Growth* **2008**, *310*, 266–269.
(8) Chen, L.; Chen, Y. B.; Wu, L. M. *J. Am. Chem. Soc.* **2004**, *126*, 16334–16335.
(9) Ding, Y.; Liu, X.; Guo, R. *Mater. Res. Bull.* **2008**, *43*, 748–758.
(10) Du, X. S.; Yu, Z. Z.; Dasari, A.; Ma, J.; Meng, Y. Z.; Mai, Y. W. *Chem. Mater.* **2006**, *18*, 5156–5158.
(11) Kuzuya, T.; Itoh, K.; Sumiyama, K. *J. Colloid Interface Sci.* **2008**, *319*, 565–571.
(12) Kuzuya, T.; Tai, Y.; Yamamuro, S.; Sumiyama, K. *Sci. Technol. Adv. Mater.* **2005**, *6*, 84–90.
(13) Lim, W. P.; Wong, C. T.; Ang, S. L.; Low, H. Y.; Chin, W. S. *Chem. Mater.* **2006**, *18*, 6170–6177.
(14) Zhang, H. T.; Wu, G.; Chen, X. H. *Langmuir* **2005**, *21*, 4281–4282.
(15) Zhang, J. Z. *J. Phys. Chem. B* **2000**, *104*, 7239–7253.

  

al. synthesized copper sulfide nanocrystals by a high temperature solution phase method.[20] Other methods like the hydrothermal approach and the aqueous colloidal capping method have also been introduced into the synthesis of copper sulfide nanoparticles.[8] Considerable efforts have been devoted to the shape controlled synthesis of nanostructured copper sulfides, various morphologies of copper sulfides have been fabricated such as nanorods,[21−24] nanotubes[4,25] nanofibers,[26] nanowhiskers,[27] nanoflakes,[28] nanowalls,[29] nanocages,[30] flowerlike,[31,32] hollow spheres,[33,34] and quadrates with varying degree of stoichiometric control.[35] The band gap of these $Cu_{2-x}S$ exhibits stoichiometry dependence. An increase in the band gap occurs with an increase of the $x$ value in bulk copper sulfides ($E_g = 1.2$ eV for $Cu_2S$, 1.5 eV for $Cu_{1.8}S$ and 2.0 eV for CuS).[36−38] Compositional control of copper sulfide nanocrystals is a way to tune the optoelectrical properties of $Cu_{2-x}S$-based materials. Reijnen and co-workers reported the fabrication of $Cu_{2-x}S$ thin films by using atomic layer deposition.[37,39] Xu et al. presented a template-assisted synthesis of well-defined $Cu_{2-x}S$ mesocages by using $Cu_2O$ crystals as sacrificial templates. The compositions of the $Cu_{2-x}S$ mesocages could be adjusted from $Cu_2S$ to $Cu_{1.75}S$ by control of the reaction conditions from a nitrogen to an air atmosphere.[40]

The difficulties in composition control, product impurities, and critical reaction conditions are the common challenges of these mentioned methods. Here, we report the novel convenient chemical synthesis of $Cu_{2-x}S$ ($x = 1$, 0.2, 0.03) nanocrystals with three different convenient and environmental benign techniques based on sonoelectrochemical,[41,42] hydrothermal,[43] and solventless thermolysis methods.[23,44] The presented methods can produce $Cu_{2-x}S$ ($x = 1$, 0.2, 0.03) nanocrystals and were used to elucidate some of the electronic and structural properties of the currently presented and some recently reported copper sulfide nanoparticles. This paper aims to address some of the existing uncertainties about the physical-chemical properties of $Cu_{2-x}S$ nanocrystals. Namely, the challenges in assignment of their X-ray and optical spectra are identified and clarified in the present work.

## Experimental Section

**Sonoelectrochemical Method.** The room-temperature sonoelectrochemical synthesis of copper sulfide nanocrystals (NCs) is based on constant-potential electrodeposition accompanied with simultaneous ultrasonication in aqueous solution.[41,42] Cupric sulfate (33 mM) was first dissolved in water and then mixed with a sodium thiosulfate solution (16.5 mM), and the citric acid concentration was 87 mM. VCX-500 ultrasonic processors from Sonics and Materials Inc. (Ti horn, 0.5 in. in diameter, 20 kHz) worked as ultrasound source and a CHI 600B electrochemistry workstation was used to control and supply a constant potential. The solution was sonicated in the presence of a constant potential in the range 0 to −1.5 V (relative to Ag/AgCl satd KCl electrode) for ∼1 h, the CuS, $Cu_{1.8}S$, and $Cu_{1.97}S$ NCs were produced at potentials 0, −0.6, and −1.2 V, respectively. After the reaction, the resulting nanocrystal suspension was centrifuged and the precipitate was washed and centrifuged three times with distilled water and ethanol.

**Hydrothermal Method.** In a three-neck flask, 1 mmol of $CuSO_4 \cdot 5H_2O$ was dissolved in 95 mL of distilled water and stirred for 15 min. Mercapto-propionic acid (MPA, 135 $\mu$L) was added into the solution under stirring. The yellow precipitate was obtained after several minutes, indicating the formation of a Cu−MPA complex. The pH value of solution was adjusted from 2 to 10 by adding 1 M NaOH solution. Then the solution was heated to 100 °C and 5 mL of 0.2 M $Na_2S_2O_3$ aqueous solution was added. The solution was refluxed at 100 °C for 7 h to produce a dark-brown precipitate. CuS and $Cu_{1.97}S$ NCs were produced at pH 2 and 5, respectively. After the reaction, the resulting nanocrystal suspension was centrifuged and the precipitate was washed and centrifuged three times with distilled water and ethanol.

**Solventless Thermolysis.** In a three-neck flask, 1 mmol of $CuSO_4 \cdot 5H_2O$ was dissolved in 100 mL of distilled water and stirred for 15 min. MPA (135 $\mu$L) was added into the solution under stirring. The yellow precipitate was separated by centrifuging and washed with water and acetone. This washing procedure was repeated three times with water and three times with acetone. The resulting precipitate was post-treated by the following two procedures.

(A) The wet precipitate was dried in air at room temperature for 3 days. The resulting green yellow powder was heated in nitrogen atmosphere at 200 °C for 60 min and cooled to room temperature. A dark-brown $Cu_{1.8}S$ powder was obtained.

(B) The wet precipitate was nitrogen-flooded for 30 min to obtain a dried waxlike gel. The resulting dried gel was heated in nitrogen atmosphere to 200 °C for 60 min and cooled to room temperature. A brown $Cu_{1.97}S$ powder was obtained.

The resulting powder was washed and centrifuged three times with water and ethanol.


(16) Yin, M.; Wu, C. K.; Lou, Y. B.; Burda, C.; Koberstein, J. T.; Zhu, Y. M.; O'Brien, S. *J. Am. Chem. Soc.* **2005**, *127*, 9506–9511.
(17) Lou, Y. B.; Yin, M.; O'Brien, S.; Burda, C. *J. Electrochem. Soc.* **2005**, *152*, G427–G431.
(18) Lou, Y. B.; Chen, X. B.; Samia, A. C.; Burda, C. *J. Phys. Chem. B* **2003**, *107*, 12431–12437.
(19) Klimov, V.; Bolivar, P. H.; Kurz, H.; Karavanskii, V.; Krasovskii, V.; Korkishko, Y. *Appl. Phys. Lett.* **1995**, *67*, 653–655.
(20) Ghezelbash, A.; Korgel, B. A. *Langmuir* **2005**, *21*, 9451–9456.
(21) Kalyanikutty, K. P.; Nikhila, M.; Maitra, U.; Rao, C. N. R. *Chem. Phys. Lett.* **2006**, *432*, 190–194.
(22) Roy, P.; Srivastava, S. K. *Mater. Lett.* **2007**, *61*, 1693–1697.
(23) Larsen, T. H.; Sigman, M.; Ghezelbash, A.; Doty, R. C.; Korgel, B. A. *J. Am. Chem. Soc.* **2003**, *125*, 5638–5639.
(24) Sigman, M. B.; Ghezelbash, A.; Hanrath, T.; Saunders, A. E.; Lee, F.; Korgel, B. A. *J. Am. Chem. Soc.* **2003**, *125*, 16050–16057.
(25) Wu, C.; Yu, S. H.; Chen, S.; Liu, G.; Liu, B. *J. Mater. Chem.* **2006**, *16*, 3326–3331.
(26) Du, W.; Qian, X.; Ma, X.; Gong, Q.; Cao, H.; Yin, J. *Chemistry* **2007**, *13*, 3241–3247.
(27) Puspitasari, I.; Gujar, T. P.; Jung, K. D.; Joo, O. S. *Mater. Sci. Eng., B* **2007**, *140*, 199–202.
(28) Zhang, H. T.; Wu, G.; Chen, X. H. *Mater. Chem. Phys.* **2006**, *98*, 298–303.
(29) Feng, X.; Li, Y.; Liu, H.; Cui, S.; Wang, N.; Jiang, L.; Liu, X.; Yuan, M. *Nanotechnology* **2007**, *18*, 145706.
(30) Xu, H. L.; Wang, W. Z.; Zhu, W.; Zhou, L. *Nanotechnology* **2006**, *17*, 3649–3654.
(31) Ji, H.; Cao, J.; Feng, J.; Chang, X.; Ma, X.; Liu, J.; Zheng, M. *Mater. Lett.* **2005**, *59*, 3169–3172.
(32) Wu, Z. C.; Pan, C.; Yao, Z. Y.; Zhao, Q. R.; Xie, Y. *Cryst. Growth Des.* **2006**, *6*, 1717–1719.
(33) Zhu, H.; Ji, X.; Yang, D.; Ji, Y.; Zhang, H. *Microporous Mesoporous Mater.* **2005**, *80*, 153–156.
(34) Ni, Y.; Liu, H.; Wang, F.; Yin, G.; Hong, J.; Ma, X.; Xu, Z. *Appl. Phys. A: Mater. Sci. Process.* **2004**, *79*, 2007–2011.
(35) Liu, Y.; Qin, D.; Wang, L.; Cao, Y. *Mater. Chem. Phys.* **2007**, *102*, 201–206.
(36) Nair, M. T. S.; Guerrero, L.; Nair, P. K. *Semicond. Sci. Technol.* **1998**, *13*, 1164–1169.
(37) Reijnen, L.; Meester, B.; Goossens, A.; Schoonman, J. *Chem. Vap. Deposition* **2003**, *9*, 15–20.
(38) Nascu, C.; Pop, I.; Ionescu, V.; Indrea, E.; Bratu, I. *Mater. Lett.* **1997**, *32*, 73–77.
(39) Reijnen, L.; Meester, B.; deLange, F.; Schoonman, J.; Goossens, A. *Chem. Mater.* **2005**, *17*, 2724–2728.
(40) Jiao, S.; Xu, L.; Jiang, K.; Xu, D. *Adv. Mater.* **2006**, *18*, 1174–1177.
(41) Qiu, X. F.; Burda, C.; Fu, R. L.; Pu, L.; Chen, H. Y.; Zhu, J. J. *J. Am. Chem. Soc.* **2004**, *126*, 16276–16277.
(42) Qiu, X. F.; Lou, Y. B.; Samia, A. C. S.; Devadoss, A.; Burgess, J. D.; Dayal, S.; Burda, C. *Angew. Chem., Int. Ed* **2005**, *44*, 5855–5857.
(43) Roy, P.; Srivastava, S. K. *Cryst. Growth Des.* **2006**, *6*, 1921–1926.
(44) Sigman, M. B.; Ghezelbash, A.; Hanrath, T.; Saunders, A. E.; Lee, F.; Korgel, B. A. *J. Am. Chem. Soc.* **2003**, *125*, 16050–16057.

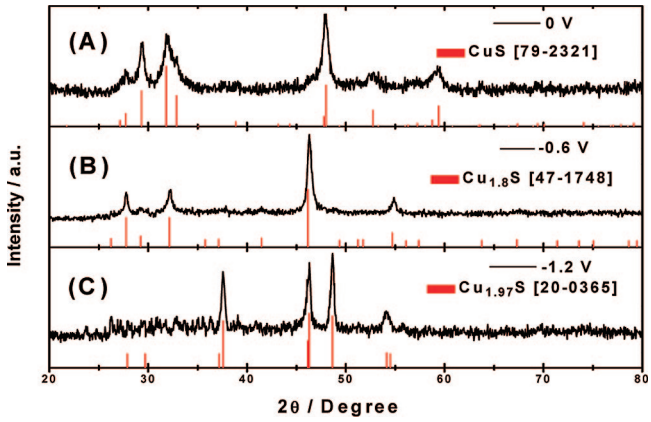


***Figure 1.*** Powder X-ray diffraction patterns of CuS (A), $Cu_{1.8}S$ (B), and $Cu_{1.97}S$ (C) nanocrystals prepared at potentials of 0, −0.6, and −1.2 V, respectively. The bars are from JCPDS standards for hexagonal CuS[79-2321], hexagonal $Cu_{1.8}S$[47-1748], and orthorhombic $Cu_{1.97}S$[20-0365].

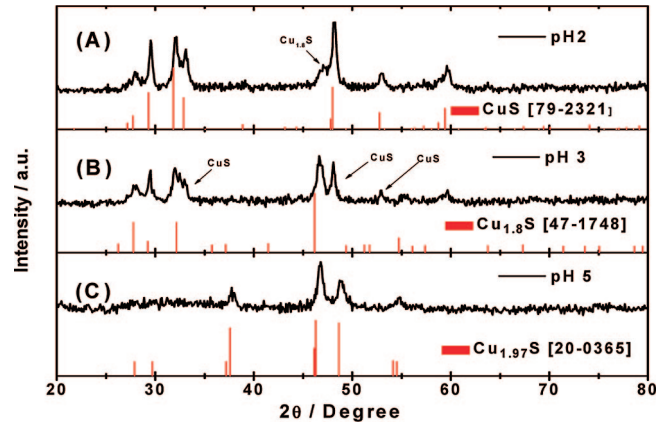


***Figure 2.*** Powder X-ray diffraction patterns of copper sulfide nanocrystals prepared by the hydrothermal method at pH 2 (A), 3 (B), and 5 (C). The bars are from standard JCPDS files of hexagonal CuS [79-2321], hexagonal $Cu_{1.8}S$ [47-1748], and orthorhombic $Cu_{1.97}S$ [20-0365]. The pattern (b) is a mixture of $Cu_{1.8}S$ and CuS.

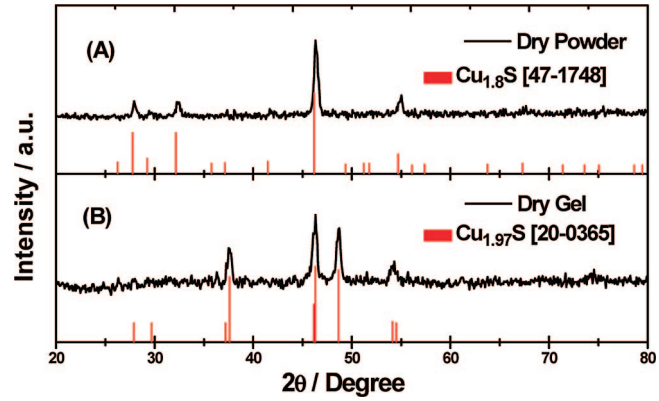


***Figure 3.*** Powder X-ray diffraction patterns of (A) hexagonal $Cu_{1.8}S$ nanocrystals by thermolysis of Cu−MPA dry powder and (B) orthorhombic $Cu_{1.97}S$ nanocrystals by thermolysis of dry Cu−MPA gel.

**Characterization.** The crystal structure of the products was examined with a Scintag X-1 Advanced X-ray powder diffractometer (XRD, 2.4°/min, Cu Kα radiation) and the morphology of these nanocrystals was characterized using a transmission electron microscope, JEOL 1200CX (TEM, accelerating voltage: 80 kV). The optical properties of the products were determined with a Varian Cary Bio50 UV−vis spectrometer. The concentrations $C_{wt}$ of the $Cu_{2-x}S$ NC dispersions for optical measurement were 0.02 g/L, and the solvent was toluene.

## Results

**Crystallinity and Morphology. Sonoelectrochemical Method.** X-ray diffraction confirmed that the sonoelectrochemical products consist of crystalline copper sulfide nanocrystals (NCs) (Figure 1). The composition control of the $Cu_{2-x}S$ has been realized by applying different potentials during the sonication. At 0 V (vs Ag/AgCl satd KCl) the resulting product is pure CuS (covellite). The obtained powder X-ray diffraction pattern (Figure 1A) matches the JCPDS reference file for CuS [79-2321]. At 0 V potential, Cu(II) in cupric sulfate does not get reduced. Only the active S(0) in sodium thiosulfate is reduced to $S^{2-}$. By lowering the work potential, the Cu(II) gets reduced to Cu(I). As a result, the diginite $Cu_{1.8}S$ NCs were produced by using a potential of −0.6 V, the corresponding XRD is shown in Figure 1B. When the reduction potential was increased to −1.2 V, a copper sulfide phase with very similar XRD to ones that others have recently reported as $Cu_2S$ nanocrystals is produced, whose standard data show peaks at 45.7° and 48.5°.[44,45] However, upon careful research and critical review of the previous reports, the XRD of the resulting copper sulfide NCs, which has peaks at 46.1° and 48.6°, have to be reassigned to $Cu_{1.97}S$ (djurleite), its standard data has peaks at 46.1°/46.3° and 48.6°. The key difference in distinguishing the $Cu_{1.97}S$ phase from $Cu_{1.8}S$ is the peak at ∼37°. On the other hand, the key difference in distinguishing the $Cu_{1.97}S$ phase from $Cu_2S$ is the peak at ∼46°. The corresponding standard JPCDS file (20-0365) is the only one that fits the experimental data. Any $Cu_2S$ standard JPCDS files did not match. With intermediate reducing potentials, mixtures of adjacent copper sulfides have been observed and confirmed by the XRD pattern. This result supported the conclusion drawn by Lambrecht et al.[6] that it is actually very difficult to make $Cu_2S$ since $Cu_{1.97}S$ is the thermodynamically stable stoichiometry under ambient reaction condition. The produced high temperature phases[6,46] also confirm that the $Cu_{2-x}S$ is formed at elevated temperature, which occurs during the micro bubble collapse during sonication.

**Hydrothermal Method.** X-ray diffraction indicated that the hydrothermal reaction of Cu−MPA with $Na_2S_2O_3$ produces crystalline copper sulfide nanocrystals (Figure 2). The compositional control of the $Cu_{2-x}S$ has been realized by adjusting the reaction solution to different pH values. At pH 2 the resulting product is mainly CuS (covellite) but one can find a weak impurity peak, which could be identified as the peak from $Cu_{1.8}S$. The obtained powder X-ray diffraction pattern (Figure 2A) is very similar to other reported XRD patterns of CuS nanocrystals.[47,48] It matches the JCPDS data files for CuS [79-2321] and $Cu_{1.8}S$ [47-1748] as mixture, as shown in Figure 2. At pH 2, the solution is acidic, the capping compound MPA is protonated, free Cu(II) ion is released from MPA. The active S(0) in sodium thiosulfate is reduced to S(2−). By increasing the pH value, the MPA is less protonated and the free Cu(II) is coordinated

(45) Liu, Z. P.; Xu, D.; Liang, J. B.; Shen, J. M.; Zhang, S. Y.; Qian, Y. T. *J. Phys. Chem. B* **2005**, *109*, 10699–10704.
(46) Chakrabarti, D. J.; Laughlin, D. E. Cu−S (Copper−Sulfur), Binary Alloy Phase Diagrams, II Ed., 1990.
(47) Roy, P.; Srivastava, S. K. *Mater. Lett.* **2007**, *61*, 1693–1697.
(48) Dixit, S. G.; Mahadeshwar, A. R.; Haram, S. K. *Colloids Surf., A* **1998**, *133*, 69–75.

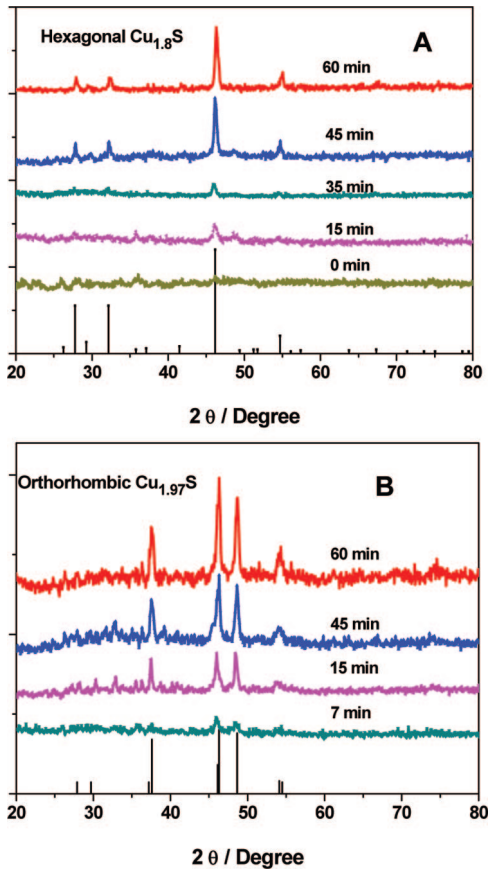


***Figure 4.*** Evolution of powder X-ray diffraction patterns of (A) $Cu_{1.8}S$ NCs synthesized via thermolysis of the Cu−MPA complex dry powder at 200 °C after different sintering times (B) $Cu_{1.97}S$ NCs synthesized via thermolysis of the Cu−MPA complex gel at 200 °C after different sintering times.

by the MPA. The lower Cu(II) ion concentration is then exposed to a relatively higher S(2−) concentration, and Cu(II) is reduced to Cu(I).[44,49] Therefore, a stronger $Cu_{1.8}S$ peak at 46° was found in the XRD of $Cu_{2-x}S$ NCs synthesized at pH 3, as shown in Figure 2B. There is a mixture of CuS and $Cu_{1.8}S$ observed when the pH value of the reaction solution is between 3 and 5. When the solution becomes less acidic and the pH increases to 5, $Cu_{1.97}S$ NCs, which match with the JCPDS 20-0365 file, have been produced. When the reaction solution becomes more basic, there is less or even no $Cu_{2-x}S$ produced. A possible reason is that the free Cu(II) ions are more chelated by the deprotonated MPA and the S(0) in sodium thiosulfate is also more difficult to release in basic solution.

**Solventless Thermolysis.** The resulting copper sulfides from solventless thermolysis of the Cu−MPA complex dry powders or dry gels in nitrogen atmosphere were also nanocrystals as confirmed by line broadening analysis using the Scherrer equation on the X-ray diffraction results (Figure 3). Thermolysis of dry powders produced diginite $Cu_{1.8}S$ NCs, matching the JCPDS 47-1748 file. On the other hand, thermolysis of dry gel produced $Cu_{1.97}S$ NCs, which matched the JCPDS 20-0365 file. The evolution of the crystallinity with thermolysis time can be tracked in Figure 4. It is found that thermolysis of dry powders needs 15 min to obtain $Cu_{1.8}S$ NCs while the thermolysis of dry gel can produce the $Cu_{1.97}S$ NCs in 7 min. Korgel et al.[23] has suggested that the mechanism of solventless synthesis of $Cu_{1.97}S$ from Cu−thiolate precursor by thermolysis is a homolytic cleavage of the thiol and alkyl groups and the Cu cations inhabit the interstitial space. At the same time, the thiols (and perhaps the carboxyl ligands) contribute to the reduction of Cu(II) to Cu(I). The selective production of $Cu_{1.97}S$ and $Cu_{1.8}S$ may come from that difference between the dry gel and dry powder of the Cu−MPA precursor. From the XRD in Figure 4, we found that the dry powder of the Cu−MPA shows some weak peaks, which indicated that the Cu−MPA dry powder has formed some crystal structure without sintering. On the other hand, the gel-like Cu−MPA precursor produced $Cu_{1.97}S$ just as reported by Korgel's[23] Cu−thiolate precursor, which do not show crystallinity without sintering.

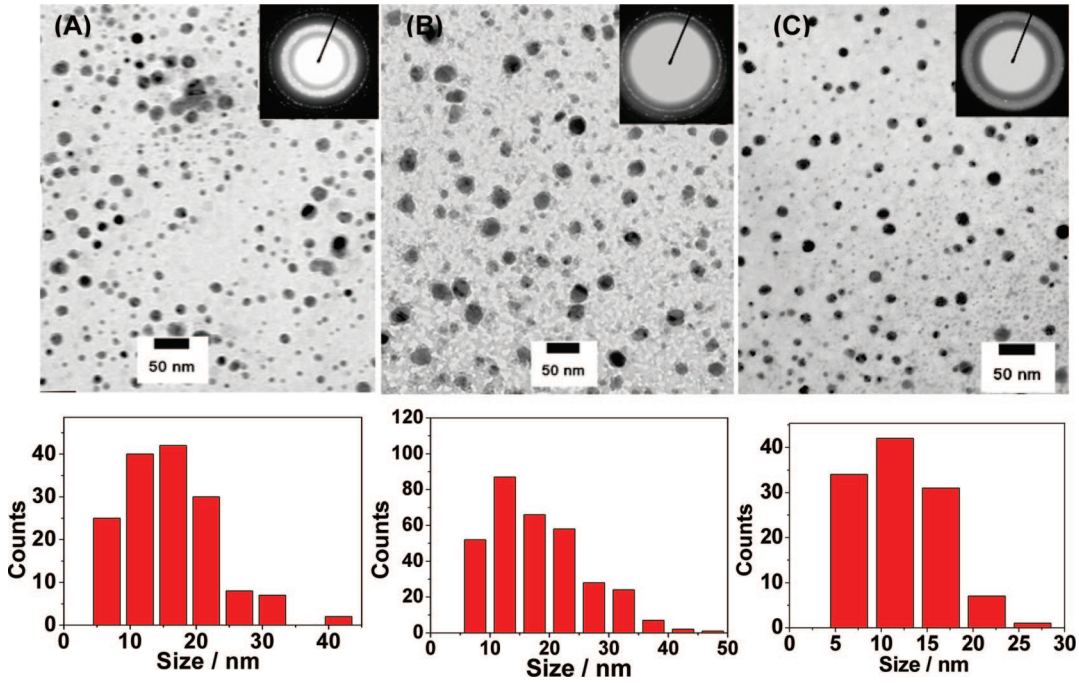


***Figure 5.*** TEM micrographs and size histograms of CuS (A), $Cu_{1.8}S$ (B), and $Cu_{1.97}S$ (C) nanocrystals synthesized by the sonoelectrochemical method.

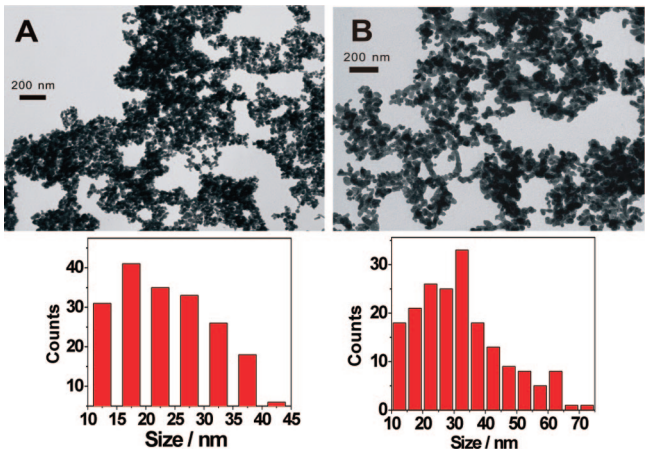


***Figure 6.*** TEM images and size histograms of of CuS NCs (A) and $Cu_{1.97}S$ NCs (B) nanocrystals synthesized by applying the hydrothermal method at pH 2 and 5, respectively.

There are a few differences between Korgel's $Cu_{2-x}S$ samples and ours that are worth considering. First, the nanocrystals presented here are bigger than the nanocrystals made by Korgel et al. Also, our $Cu_{1.97}S$ nanocrystals do not have a disk shape. This shape was one of the factors Korgel et al.[23] considered when determining the crystal structure and it led to the conclusion that their nanocrystals could be hexagonal $Cu_2S$.

Consistent with our results, Korgel could produce CuS disks in solution, and also made some of the nonstoichiometric phases, but not $Cu_2S$. So, there might be something particular about the solventless reaction conditions. At least they have a significant influence over the copper sulfide stoichiometry.

The size and shape of the sonoelectrochemically synthesized copper sulfide NCs are shown in Figure 5. The particle sizes of these $Cu_{2-x}S$ are within a range of 5−20 nm. The particle shape of the various copper sulfide NCs are similar. For the CuS NCs (A), the particle sizes are 14.9 ± 7.1 nm; for the $Cu_{1.8}S$ NCs (B) the particle sizes are 18.1 ± 7.9 nm; for the $Cu_{1.97}S$ NCs (C) the particle sizes are 12.1 ± 4.6 nm. The average size was counted by ImageJ software for more than 100 particles. The size of these nanoparticles, as calculated by the Scherrer equation on the basis of the three most intense peaks, is about 15, 16, and 18 nm for CuS (A), $Cu_{1.8}S$ (B), and $Cu_{1.97}S$ (C), respectively, which is in reasonable agreement with the TEM results.

The size and shape of the hydrothermally synthesized $Cu_{2-x}S$ NCs are shown in Figure 6. For the CuS NCs (A) the particle sizes are 22.3 ± 8.2 nm; for the $Cu_{1.97}S$ NCs (B) the particle sizes are 30.3 ± 12.6 nm. The average size was measured by randomly counting 200 particles in the images. The size of these nanoparticles, as calculated by the Scherrer equation on the basis of the three most intense peaks, is about 20 and 22 nm for CuS (A) and $Cu_{1.97}S$ (B), respectively, in reasonable agreement with the TEM results. These particles appear on the TEM grid aggregated to each other, which may come from the use of MPA as ligand.

The size and shape of the thermolysis synthesized copper sulfide NCs are shown in Figure 7. For the $Cu_{1.8}S$ NCs (A), via thermolysis of the dry Cu−MPA powder, the particle sizes are

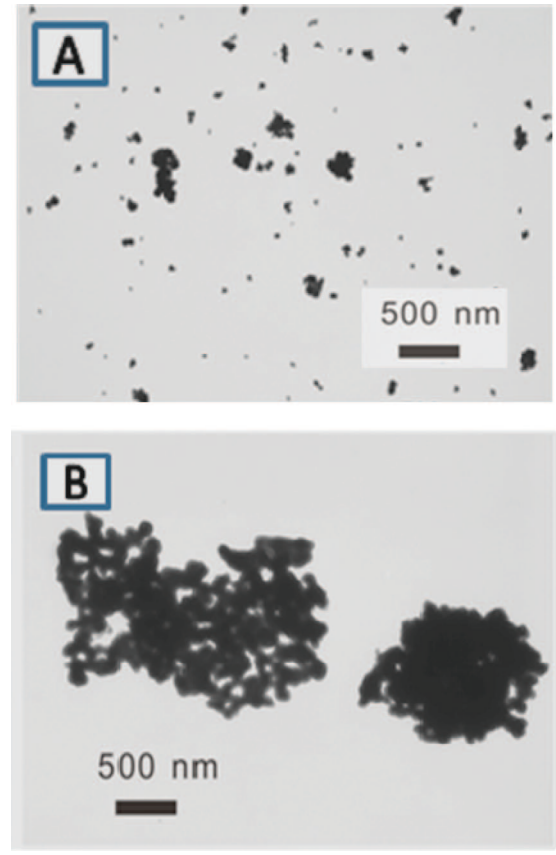


***Figure 7.*** TEM images of $Cu_{1.8}S$ NCs synthesized by solventless thermolysis of a dry powder (A) and $Cu_{1.97}S$ NCs synthesized by solventless thermolysis of a dry gel (B).

51.2 ± 20.6 nm, as counted by ImageJ software. For the $Cu_{1.97}S$ NCs (A), via thermolysis of the Cu−MPA gel, these particles are aggregated on the TEM grid to form larger agglomerates when the solution dries. The TEM shows that the NC size of $Cu_{1.8}S$, from thermolysis of the dry Cu−MPA powder, is smaller than the obtained $Cu_{1.97}S$ NCs, from thermolysis of the Cu−MPA gel, and the $Cu_{1.8}S$ NCs seem to be better dispersed. The difference comes possibly from the crystal-like property of the dry powder precursor, which breaks into small particles when thermolyzed, while the $Cu_{1.97}S$ NCs from the gel-like precursor tends to stay agglomerated after the transformation from the amorphous precursor into crystalline $Cu_{1.97}S$ NCs. The size of these nanoparticles, as calculated by the Scherrer equation on the basis of the three most intense peaks, is about 26 and 30 nm for CuS (A) and $Cu_{1.97}S$ (B), respectively, This is significantly different from the TEM result for the $Cu_{1.97}S$ NCs. The difference may come from the heavy agglomeration during the thermolysis process.

**UV−Vis Absorption Spectra.** In this work we synthesized $Cu_{2-x}S$ NCs with three new methods in order to compare structural, compositional and optical properties between these $Cu_{2-x}S$ NC samples. The comparison will then be extended to the existing literature about $Cu_{2-x}S$ NCs. The UV−vis absorption spectra of the differently made $Cu_{2-x}S$ NCs are shown in Figure 8. By estimating a molar NC concentration $C$ and measuring the experimental absorbances, one can obtain a good estimate for the extinction coefficient $\varepsilon(\lambda)$of these NCs.

The molar concentration $C$ of the nanocrystal dispersion is calculated by eq 1

(49) Silvester, E. J.; Grieser, F.; Sexton, B. A.; Healy, T. W. *Langmuir* **1991**, *7*, 2917–2922.

$$C = C_{wt}/M_{NC} = C_{wt}/\left(\frac{\pi}{6}d^3\rho N_A\right) \quad (1)$$

$C_{wt}$ is the weight concentration of the nanocrystals, $M_{NC}$ is the molar weight of the nanocrystals, $N_A$ is Avogadro's constant, $d$ is the average diameter of the nanocrystals assuming the nanocrystals are spherical, and $\rho$ is the density of the nanocrystals assuming it is the same as bulk. The extinction coefficient could be calculated from the measured absorbance $A$ in eq 2

$$\varepsilon = \left(A\frac{\pi}{6}d^3\rho N_A\right)/(LC_{wt}) \quad (2)$$

The density $\rho$ for $Cu_{2-x}S$ is about 5.6 g/cm$^3$. On the basis of the TEM and XRD results, we assume that the diameters for CuS, $Cu_{1.8}S$, and $Cu_{1.97}S$, synthesized by the sonoelectrochemical method, are 15 nm. For CuS and $Cu_{1.97}S$, synthesized by the hydrothermal method, the diameters are assumed to be 25 nm, for $Cu_{1.8}S$ and $Cu_{1.97}S$, synthesized by the thermolysis method, the diameters are assumed to be 30 nm. The so obtained extinction coefficients $\varepsilon(\lambda)$ from measured absorbances $A$ for each sample are shown in figure 8.

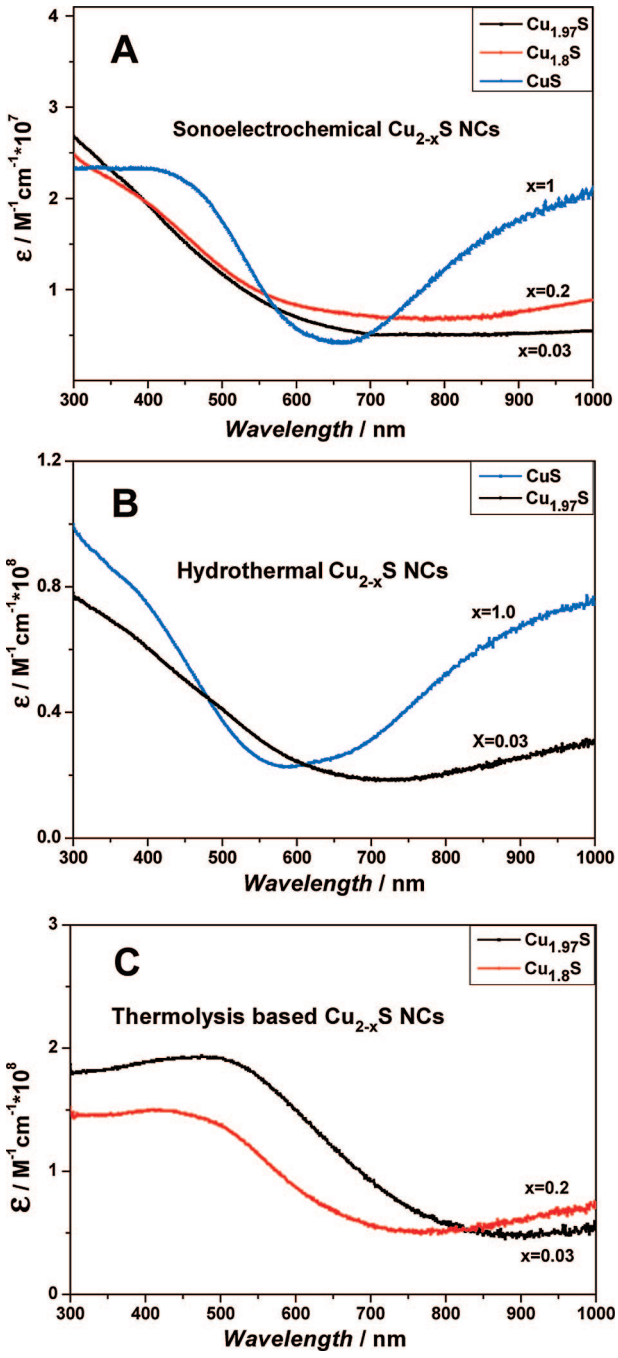


***Figure 8.*** UV−vis spectra of $Cu_{2-x}S$ NCs prepared by (A) sonoelectrochemical, (B) hydrothermal, and (C) thermolysis methods.

**Sonoelectrochemical.** The spectra of the sonoelectrochemically synthesized $Cu_{2-x}S$ NCs are shown in Figure 8A, the absorbance of $Cu_{1.8}S$ and $Cu_{1.97}S$ NCs of ~15 nm diameter has a shoulder at ~400 nm, which is similar to previously reported 10−20 nm CuS NCs,[50,51] and reaches a minimum at ~800 nm. On the other hand, the absorbance never reaches zero intensity but rises for longer wavelengths again, which is thought to come from the free-carrier intraband absorbance.[4] The absorbance of CuS NCs has a broad shoulder around 450 nm and reaches a minimum around 650 nm, but again not zero intensity. It rises for longer wavelengths stronger than the $Cu_{1.8}S$ and $Cu_{1.97}S$ NCs due to free-carrier absorbance.[4]

**Hydrothermal.** The spectra of hydrothermally synthesized $Cu_{2-x}S$ NCs are shown in Figure 8B. The ~25 nm $Cu_{2-x}S$ NCs, hydrothermally synthesized at pH 2, were assigned to mainly CuS and a little $Cu_{1.8}S$ on the basis of their XRD patterns. They show an absorbance around 400 nm and a strong absorbance at long wavelength, which arises on the basis of free carrier intraband absorption.[4,50,51] However, the spectrum of the hydrothermally synthesized $Cu_{2-x}S$ NCs at pH 5, which is assigned to $Cu_{1.97}S$, shows a broad absorbance from 300 to 600 nm, similar to previously reported 10 nm $Cu_{2-x}S$.[49] Both of these two hydrothermally synthesized $Cu_{2-x}S$ reach a minimum around 600 nm then rise for longer wavelengths due to free carrier intraband absorption.[4] Generally, we find that CuS NCs show a stronger free carrier absorbance than the other $Cu_{2-x}S$ NC compositions, consistent with recently reported spectra of CuS NCs.[45,47,48]

**Thermolysis.** The spectra of $Cu_{2-x}S$ NCs synthesized via thermolysis, which were assigned to 30−70 nm $Cu_{1.8}S$ and $Cu_{1.97}S$, are shown in Figure 8C. The absorbance of $Cu_{1.97}S$ NCs shows a broad maximum from 400 to 650 nm, which is about 50 nm red-shifted compared to $Cu_{1.97}S$ NCs made via sonoelectrochemical and hydrothermal methods. The absorbance of $Cu_{1.8}S$ NCs also shows a broad peak from 400 to 650 nm, which is about 70 nm red-shifted compared to $Cu_{1.8}S$ NCs made via sonoelectrochemistry. Both spectra of these two thermolysis-based $Cu_{2-x}S$ NCs reach a minimum at around 800 nm and then increase in intensity for longer wavelengths due to free-carrier absorbance.[4] The quantum size effect for the thermolysis-based $Cu_{1.8}S$ and $Cu_{1.97}S$ NCs was less than for the corresponding NCs synthesized via the sonoelectrochemical and the hydrothermal method, which can be rationalized on the basis of the different size ranges.

From the UV−vis spectra for these $Cu_{2-x}S$ NCs, we find long wavelength absorbance for all presented stoichiometries ($x \neq 0$). Since this NIR absorbance derives from free carriers, it should show a stoichiometric dependence. CuS NCs show very strong absorbance intensity, while the $Cu_{1.8}S$ NCs show somewhat less absorbance and the $Cu_{1.97}S$ NCs show further decreased absorbance intensity in the NIR region. We could identify comparable trends in previously published work for bulk

(50) Ding, T. Y.; Wang, M. S.; Guo, S. P.; Guo, G. C.; Huang, J. S. *Mater. Lett.* **2008**, *62*, 4529–4531.
(51) Zhang, H. T.; Wu, G.; Chen, X. H. *Mater. Chem. Phys.* **2006**, *98*, 298–303.

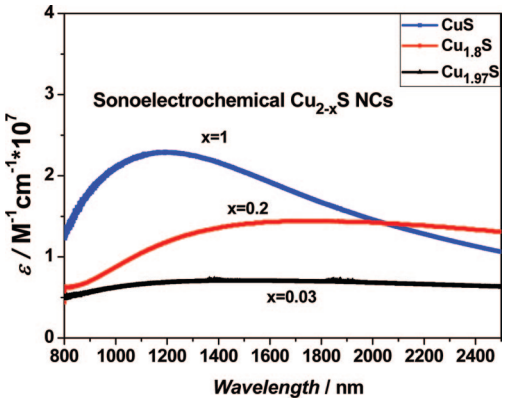


***Figure 9.*** NIR spectra of prepared $Cu_{2-x}S$ NCs: CuS ($x = 1$), $Cu_{1.8}S$ ($x = 0.2$), and $Cu_{1.97}S$ ($x = 0.03$) synthesized by the sonoelectrochemical method. Relative spectral intensities are shown as measured and overlapped with Figure 8A to obtain extinction coefficients for the NIR region.

$Cu_{2-x}S$ materials.[48] The similarity of the spectra (for similarly sized NCs) is quite consistent. It is shown here that the optical properties are largely independent of the synthesis procedure. Furthermore, a comparison between panels A and C in Figure 8 shows a size dependence effect, and a systematic size dependence study is planned for the future. Figure 9 shows that $Cu_{2-x}S$ NCs have comparable NIR absorption spectra. They show that the NIR absorption intensity increases with increasing $x$, identical to the red end of the UV−vis spectra in figure 8 in which CuS shows the strongest NIR absorption followed by $C_{1.8}S$ and then by $Cu_{1.97}S$ with the lowest absorption intensity above 800 nm. Note that for perfect $Cu_2S$ the valence band is filled and free carrier absorption would not occur. This is an unambiguous way to distinguish $Cu_2S$ from $Cu_{2-x}S$.

## Discussion

**Structural Properties.** XRD is a powerful characterization method to determine the crystal phase of materials. Most reported nanocrystalline materials were determined via their crystal structure because the XRD pattern for any of these materials is unique and significantly different from any other materials. However, there are a total of 86 reported XRD patterns for $Cu_{2-x}S$ and the different stoichiometric copper sulfides have very similar XRD patterns, which makes the assignment of copper sulfide XRDs very tedious. Phase diagrams[46] help additionally in assigning the investigated materials. For example, the $Cu_2S$ (chalcocite) and $Cu_{1.97}S$ (djurleite) have similar XRD pattern, and the phase space of $Cu_2S$ is very narrow compared to $Cu_{1.8}S$ in the phase diagram.[46] This explains some inconsistency in recent literature between some reported assignments of $Cu_{2-x}S$ materials and the reported standard XRD files. The fact that all three methods we used can produce $Cu_{1.97}S$ but can not produce $Cu_2S$ under ambient conditions is consistent with the reported result that $Cu_2S$ has a thermodynamic instability toward copper-deficient copper sulfide phases and favors the formation of copper vacancies even in contact with pure copper.[6] Very recently Alivisatos et al.[53] prepared $Cu_2S$ NCs under Ar protection.

It is important to point out here that, while these three XRD patterns are very similar, they are, after careful study, distinguishable. For example the XRD of the $Cu_{1.97}S$ distinguishes itself from the $Cu_2S$ XRD with very narrow double peaks at 37.1°, 46.1°/46.3°, and 54.1°. While these peaks can be weak and broad and overlooked in an experimental diffraction pattern, it is the distance between the strong peaks at 46.1°/46.3° and 48.6°, which uniquely identifies $Cu_{1.97}S$; $Cu_2S$ has strong peaks at 45.7° and 48.5°. Comparison of these files with the literature suggests that $Cu_2S$ is actually not produced under ambient conditions. At least for any $Cu_{2-x}S$ synthesized under ambient conditions without Ar protection, the XRD analysis of "$Cu_2S$" should be revisited.

Lambrecht's theoretical study has shown that the $Cu_2S$ will be a monoclinic structure at low temperature,[6] the hexagonal form is stable in the range of 103−436 °C and the cubic structure forms at high temperature.[54] However, hexagonal $Cu_2S$ was not observed in any of our attempts, based on the XRD. Instead, the orthorhombic djurleite $Cu_{1.97}S$ XRD pattern was observed. This indicated that the $Cu_{2-x}S$ changes its crystal structure from $Cu_2S$ to $Cu_{1.97}S$ as a result of copper loss from $Cu_2S$ and minor rearrangements of the sulfur atoms.[55] An XRD pattern consistent with standard JPCD files of $Cu_2S$ was published recently by Alivisatos et al.[53]

While it is very interesting that one finds a better match with $Cu_{1.97}S$ (djurleite) XRD patterns for nanomaterials that were previously assigned as $Cu_2S$ (chalcocite),[19,41,42,44,52] one should not be too focused on these crystallographic assignments, which probably have historical origins in mineralogy applications. It rather shows that $Cu_{2-x}S$ varies with a continuous $x$ and the structural changes and names between different $x$ are difficult to determine and probably not very meaningful given that there is a good deal of disorder in all these compositions.[6] On the other hand, knowing the 86 existing diffraction patterns for $Cu_{2-x}S$ and being able to assign them to the synthesized materials helps to determine a phase and with that a compositional range.

**Optical Properties.** UV−vis absorption spectra of various $Cu_{2-x}S$ materials have been published earlier.[11,19,45,47,51] However, they appear in the majority of recent publications without context in size dependence or composition. Reason for this lack of analysis of the spectra is probably the initial wrong assignment in the pioneering work as indirect band gap material, which derives from a questionable approach to analyze the band gap transition.[4] In this early work the long-wavelength absorption (Drude term) was truncated and neglected, which lead to substantial arbitrariness to assign the band gap transitions as indirect ones. Lambrecht's work[6] implied that the absorption of hexagonal $Cu_{2-x}S$ is (a) direct band gap, (b) a function of $x$, due to the underlying Moss−Burstein effect,[56,57] in which increasing doping (increasing $x$) will lead to an increase of hole formation in the valence band and effectively lower the energy of the lowest occupied energy level, (c) size-dependent in the 10 nm particle range. From Lambrecht's theoretical study, the approximate exciton mass $\mu_x$ for copper sulfide is 0.2 from using eq 3 with the effective electron mass ($m_e$) and corresponding effective hole mass ($m_h$).[6]

(52) Zhuang, Z.; Peng, Q.; Zhang, B.; Li, Y. *J. Am. Chem. Soc.* **2008**, *130*, 10482–10483.
(53) Will, G.; Hinze, E.; Rahman, A.; AbdelRahman, M. *Eur. J. Mineral.* **2002**, *14*, 591–598.
(54) Whiterside, S. L.; Goble, J. R. *Can. Mineral* **1986**, *24*, 247–258.
(55) Wu, Y.; Wadia, C.; Ma, W.; Sadtler, B.; Alivisatos, A. P. *Nano Lett.* **2008**, *8*, 2551–2555.
(56) Moss, T. S. *Proc. Phys. Soc. B* **1954**, *67*, 775–782.
(57) Burstein, E. *Phys. Rev.* **1954**, *93*, 632–633.

$$\frac{1}{\mu_x} = \frac{1}{m_e} + \frac{1}{m_h} \quad (3)$$

In comparison, the well-studied material CdSe has an excition mass $\mu_x = 0.1$, and the exciton Bohr radii for CdSe is 5.3 nm.[58] One can obtain an exciton Bohr radius for $Cu_{2-x}S$ of about 3−5 nm by using the equation for the excitonic Bohr radius $a_B = \varepsilon/\mu_x$ if one assumes that the relative dielectric constant $\varepsilon$ for copper sulfides is about 10−15. This will likely be a function of the composition in $Cu_{2-x}S$ and a dielectric constant 10−15 seems reasonable for small $x$ compared to other semiconductor materials.[58] The size effect range for CdSe QD is from 1−6 nm. Similarly, we expect to see a strong quantum size effect for $Cu_{2-x}S$ in the sub-10 nm range. In agreement with this analysis, several reported $Cu_{2-x}S$ NCs show blue-shifted band gap absorption compared to bulk material, while their sizes are in the 10 nm region.[45,59,60] However, the dielectric constant may even be larger than these regular values because of the free carriers in these nonstoichiometric $Cu_{2-x}S$, which leads to larger Bohr radii and broader quantum size ranges. For example PbTe has a dielectric constant of ∼100 due to its narrow band gap energy and a Bohr radius of ∼50 nm.[61,62] The dielectric constant of $Cu_{2-x}S$ could well depend on $x$ and reach high values for compositions with larger $x$ values. This would accordingly increase the exciton bohr radii by an order of magnitude. Indeed, the large blue-shifts observed in Figure 8 and the consistently underestimated band gap energies by theory[6] strongly hint toward large exciton Bohr radii and dielectric constants for $Cu_{2-x}S$ nanomaterials. To the best of our knowledge, these basic properties are to date undetermined for copper deficient $Cu_{2-x}S$.

All UV−vis spectra of the synthesized copper sulfide NCs show a broad blue-shifted peak around 400−600 nm, indicating size quantization effects, which has been reported earlier for the case of $Cu_{2-x}S$ NCs.[5,63] On the other hand, the UV−vis spectra of $Cu_{2-x}S$ NCs do not show strong compositional dependence as was reported for bulk copper sulfide.[37] A possible reason for this is that the quantum size effect in these $Cu_{2-x}S$ prevails over the band gap changes due to the Moss−Burstein effect.[56,57] This can be confirmed by the fact that a more significant blue-shift is observed in the 5−20 nm $Cu_{2-x}S$ NCs synthesized via sonoelectrochemical and hydrothermal methods compared to the 20−70 nm $Cu_{2-x}S$ NCs, which were synthesized via thermolysis. The obtained experimental extinction coefficient $\varepsilon$ for these synthesized $Cu_{2-x}S$ NCs in the region of $10^7-10^8$ $M^{-1}$ $cm^{-1}$confirms that these materials should all be of direct band gap character.

**Plasmonic NIR Absorption.** The NIR absorption of these $Cu_{2-x}S$ NCs can be interpreted in terms of valence band free carriers, which are essentially metallic in character and give rise to a Drude term with corresponding NIR plasmon absorption (Figure 9). Metals provide the best evidence of plasmons, because they have a high density of free electrons. In the presented $Cu_{2-x}S$ nanoparticles, the majority charge carriers are positive holes. The frequency of a plasma-wave oscillation is determined by the carrier density and the energy of the corresponding plasmon is its frequency multiplied by Planck's constant ($h$).

From Mie theory, the extinction coefficient for $N$ particles of volume $V$ is given by the following equation.[64,65]

$$\kappa_{ext}(\lambda) = 18\pi NV\varepsilon_m^{3/2}\frac{\varepsilon_2(\omega)}{\lambda[(2\varepsilon_m + \varepsilon_1(\omega))^2 + \varepsilon_2(\omega)^2]} \quad (4)$$

Where $\varepsilon_1(\omega)$ and $\varepsilon_2(\omega)$ are the real and imaginary parts of the dielectric constant, respectively, $\varepsilon_m$ is the dielectric constant of the surrounding medium.

From the Drude theory, $\varepsilon_1(\omega)$ and $\varepsilon_2(\omega)$ is given by following equations

$$\varepsilon_1(\omega_p) = \varepsilon_{core} - \frac{4\pi ne^2\tau^2}{m^*(1 + \omega_p^2\tau^2)} \varepsilon_2(\omega_p) = \frac{4\pi}{m^*\omega_p}\frac{ne^2\tau}{1 + (\omega_p\tau)^2} \quad (5)$$

Where $\omega_p$ is the plasma frequency, $e$ is the elementary charge, $n$ is the free carrier (hole for the $Cu_{2-x}S$) concentration, $\varepsilon$ is the dielectric constant, $m^*$ is the charge carrier effective mass and $\tau$ is the average relaxation time.

The plasmon resonance condition is $2\varepsilon_m + \varepsilon_1 = 0$ if $\varepsilon_2(\omega)$ is small or only weakly dependent on $\omega$.[65] One can obtain $\omega_p$ from eq 5

$$\omega_p^2 = \frac{4\pi ne^2}{m^*(2\varepsilon_m + \varepsilon_{core})} - \frac{1}{\tau^2} \approx \frac{4\pi ne^2}{m^*(2\varepsilon_m + \varepsilon_{core})} \quad (6)$$

It is shown in eq 6 that the plasmon frequency $\omega_p$ increases with free carrier concentration ($n^{1/2}$). In other words, the resonance wavelength $\lambda$ will decrease with increasing $x$ in $Cu_{2-x}S$, as is observed in Figure 9.

At plasmon resonance, $2\varepsilon_m + \varepsilon_1 = 0$,[65] the extinction coefficient eq 4 can be simplified by using eqs 5 and 6 and $\omega_p^2\tau^2 \gg 1$ for optical to NIR frequencies

$$\kappa_{ext}(\lambda) = \frac{18\pi NV\varepsilon_m^{3/2}}{\lambda}\frac{m^*\omega_p^3\tau}{4\pi ne^2} = \frac{18NV\varepsilon_m^{3/2}\tau}{\lambda}\frac{(4\pi ne^2)^{1/2}}{m^{*1/2}(2\varepsilon_m + \varepsilon_{core})^{3/2}} \quad (7)$$

From eq 7, one finds that the extinction coefficient $\kappa_{ext}(\lambda)$ at wavelength $\lambda$ increases with the free carrier concentration $n^{1/2}$ (i.e., increasing $x$) assuming constant $N$ and $V$ for the investigated $Cu_{2-x}S$ NPs samples. This is also directly observed in Figure 9. For perfect nonoxidized $Cu_2S$ NPs, such a plasmon absorbance would not exist, which is supported by very recent work of Alivisatos et al.[55] and we could confirm that the absorbance of so prepared $Cu_2S$ NCs starts to show long wavelength absorbance after the $Cu_2S$ NCs were exposed to air.

## Conclusion

In summary, we have synthesized a series of compositionally controlled $Cu_{2-x}S$ nanocrystals via three novel different chemical procedures using sonoelectrochemical, hydrothermal, and thermolysis methods. The range of compositions of the $Cu_{2-x}S$ nanocrystals ranged from CuS (covellite) to $Cu_{1.97}S$ (djurleite) through adjusting the reduction potentials from 0 to −1.2 V in

(58) Fu, H. X.; Wang, L. W.; Zunger, A. *Phys. Rev. B* **1999**, *59*, 5568–5574.
(59) Roy, P.; Srivastava, S. K. *J. Nanosci. Nanotechnol.* **2008**, *8*, 1523–1527.
(60) Behboudnia, M.; Khanbabaee, B. *J. Cryst. Growth* **2007**, *304*, 158–162.
(61) Kanai, Y.; Shohno, K. *Jpn. J. Appl. Phys.* **1963**, *2*, 6–10.
(62) Wise, F. W. *Acc. Chem. Res.* **2000**, *33*, 773–780.
(63) Haram, S. K.; Mahadeshwar, A. R.; Dixit, S. G. *J. Phys. Chem.* **1996**, *100*, 5868–5873.
(64) Papavassiliou, G. C. *Prog. Solid State Chem.* **1980**, *12*, 185–286.
(65) Link, S.; El-Sayed, M. E. *J. Phys. Chem. B* **1999**, *103*, 8410–8426.

the sonoelectrochemical method, from CuS to $Cu_{1.97}S$ (djurleite) by adjusting the pH values from 2 to 5 in the hydrothermal method and from $Cu_{1.8}S$ to $Cu_{1.97}S$ in the thermolysis method. On the basis of these results, the $Cu_2S$ is found to be thermodynamically unstable under ambient condition, compared to the copper deficient $Cu_{2-x}S$ phase. The UV−vis interband spectra of the synthesized $Cu_{2-x}S$ NCs show a blue shift in the absorption compared to bulk (a) due to a quantum size effect and (b) a Moss−Burstein effect caused by the copper deficiency in $Cu_{2-x}S$. The intensity of the observed spectra show that all studied $Cu_{2-x}S$ nanocrystals should be of direct band gap type. The observed properties of the synthesized $Cu_{2-x}S$ nanocrystals are in accordance with recent calculations by Lambrecht et al. The NIR spectra of these $Cu_{2-x}S$ NCs show a plasmonic absorption, which is carrier concentration dependent.

**Acknowledgment.** C.B. gratefully acknowledges financial support from NSF (CHE-0239688), NIRT (0608896), and ACS PRF (45359-AC10). J.J.Z. is financially supported by the National Natural Science Foundation of China (20635020, 20325516).

JA805655B